Romanian Reports in Physics, Vol. 60, No. 1, P. 157–171, 2008

APPLICATION OF DYNAMIC PROGRAMMING TO THE DATING OF A LOESS-PALEOSOL SEQUENCE⋆

C. NECULA, C. PANAIOTU

University of Bucharest, Faculty of Physics, Bucharest, Romania (c3necula@yahoo.com)

(Received November 14, 2006)

Abstract. Several time series were generated using dynamic programming by tuning magnetic susceptibility to 65°N insolation curve and to a stack of benthic $\delta^{18}O$ records. The most straightforward time scale was obtained by benthonic oxygen matching. This result shows that the global ice volume had a higher influence on the magnetic susceptibility than insolation forcing.

Key words: orbital tuning, loess-paleosol, magnetic susceptibility, Milankovich periodicities.

1. INTRODUCTION

Magnetic susceptibility of loess-paleosol sequences from the temperate northern hemisphere successfully record the glacial-interglacial paleoclimatic cycles of the Quaternary. Reliable reconstruction of history for such paleoclimatic fluctuations requires generation of accurate age models for loess deposits. Recent studies provide good examples for timescale development based on orbital tuning of magnetic susceptibility [1, 2, 3, 4]. Spectral analysis of these time series shows that periods in the range 100, 41, 23 and 19 kyr are significantly present over the last 500 kyr providing substantial evidence that, at least near the frequencies of variations in obliquity and precession, a fraction of the climatic variance is driven by insolation changes. The variance components centered near 100ky dominate most upper Pleistocene climatic records more or less in phase with the eccentricity cycle, [5], or lagging it, [6]. Milankovich theory, however, has come recently under question, [7, 8, 9, 10, 11, 12]. To understand long-term climate changes it is, thus, necessary to investigate more deeply these methods of orbital tuning.

Recent results [13] have shown that magnetic susceptibility from the Mostistea loess-paleosol section displays variations similar to those from Chinese loess sections, with lower susceptibility values in loess during glacial periods and higher values in paleosols during interglacial periods. Based on this climatic

⋆ Paper presented at the Annual Scientific Conference, May 26, 2006, Faculty of Physics, Bucharest University, Romania.

control, [14] developed an astronomical age model using the method of [2]. Spectral analysis of the obtained time series has shown the main Milankovich periodicities (100, 41, 23 and 19 ky). In this paper our aim is to test the ability of the dynamic programming method [17] to generate time series for magnetic susceptibility from the Mostistea loess-paleosol deposit using as target curves the 65°N summer insolation [15] and the stack of 57 globally distributed benthic $\delta^{18}O$ records [16].

2. METHOD

The loess-paleosol profile is situated on the border of the Mostistea lake (Danube plain, SE Romania: 44.16°N 26.83°E). It consists of four loess horizons (L1, L2, L3, L4), three interbedded paleosols (S1, S2, S3) and recent soil (S0). According to [14], from IRSL (infrared stimulated luminescence) measurements, each paleosol correspond to an interglacial cycle and even marine isotope stage (MIS): S1 – MIS5, S2 – MIS7, S3 – MIS9 and S4 – MIS11. Each loess layer corresponds to a glacial cycle and odd MIS: L1 – MIS2-4, L2 – MIS6, L3 – MIS8 and L4 – MIS10.

We have generated several time series for magnetic susceptibility using Match-2.0.1 software [17] for two target curves: the 65°N summer insolation curve [15] and the stack of 57 globally distributed benthic $\delta^{18}O$ records [16].

The time scale for benthic $\delta^{18}O$ records was established by [16] using a simple nonlinear model of ice volume, y, which follows the equation

$$\frac{dy}{dt} = \frac{1 \pm b}{T_m}(x - y),$$

where b is the nonlinearity coefficient which is subtracted during ice growth and added during ice decay, T_m is the mean time constant of the ice model and x is the 21 June insolation curve for 65°N calculated by [18].

The Match-2.0.1 software is based on the dynamic optimization method which consists in matching automatically two series by dividing each of the series into many small intervals and calculates an alignment score for each possible mapping of these intervals. The technique constrains the sequential ordering of the intervals, ensuring that the derivative of the matching function is not negative. The score of each mapping is primarily determined by the square of the difference between the two signals, [17]. The software allows 3 types of matching: forced, unforced and with tie points.

Spectral and wavelet analysis of the magnetic susceptibility time series was performed with Spectrum, [19], and Nuspectral, [20], respectively.

3. RESULTS AND DISCUSSIONS

3.1. ORBITAL TUNING

In the first numerical experiment all time series were obtained forcing the program to match the start and end points of the signal with the start and end points of the target curves. Because our loess-paleosol sequence end at the base of a paleosol, the insolation curve was cut at the values corresponding to accepted ages of paleosols bases [2] (*e.g.*, 129 kyr, 250 kyr, 342 kyr, etc. which correspond to paleosols S1, S2, S3, etc. bases).

The results of the tuning procedure between magnetic susceptibility and 65°N summer insolation curve are shown in Fig. 1. These time-depth curves show that two solutions fit the IRSL ages corresponding to end points at 342 or 417 kyr. Discrimination between these two solutions comes from the characteristics of the paleosol S3. This paleosol is not a double paleosol in none of the loess deposits from Romania and adjacent areas: Primoskoje (Ukraine) [21]; Nova Etuliya and Roxolany (Ukraine) [22]; Koriten (Bulgaria) [23]; Paks (Hungary) [24]). The same is true for distant loess deposits from China, [1, 2, 25], and Central Asia, [3]. Based on this field observation we think that the best solution correspond to the end point at the base of paleosol S4 (417 ka).

In the second numerical experiment we have generated new time series matching without any constrains the magnetic susceptibility curve and with the insolation curve cut at 342 kyr and 433 kyr. We have chosen to cut the insolation

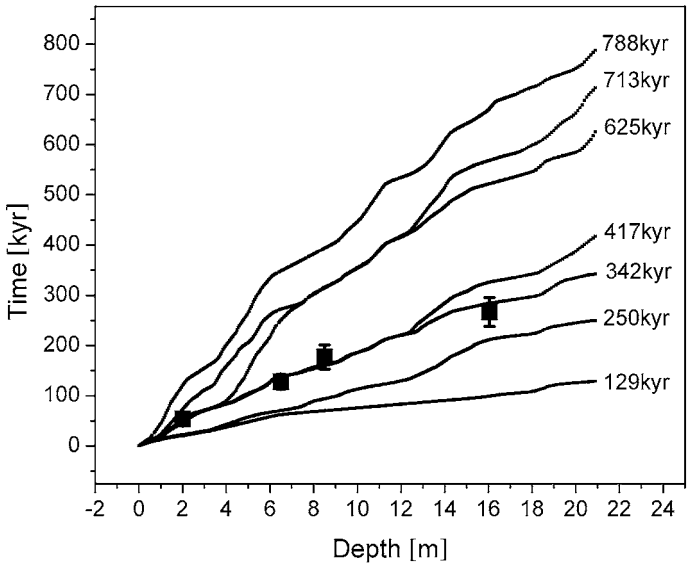

Fig. 1 – Comparison of astronomical dating (black lines) and IRSL ages (black squares) with confidence limits.

curve at 433 kyr for this second experiment because the end point of magnetic susceptibility curve is in a loess layer. According to [2], such a point must be assigned to a minimum in insolation which is around 433 kyr. The age-depth curves shows (Fig. 2a) that 433 kyr time series is completely out of range with respect to IRSL ages, indicating an age for Mostistea section of 342 kyr. However the correlation curves (Fig. 3) display a wrong match with both 342 and 417 kyr

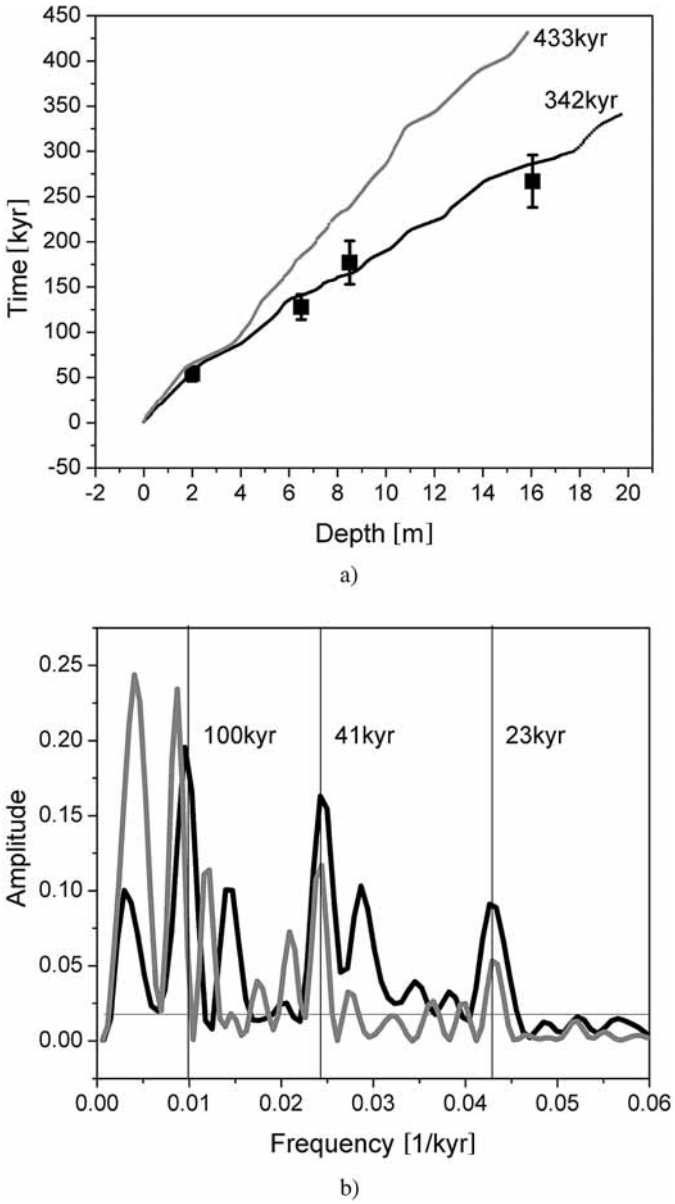

Fig. 2 – (a) Comparison between the two time scales (black line = 433kyr length time series, gray line = 342 length time series) obtained with the unforced program and IRSL ages (black squares) with confidence limits. (b) Power spectra of the same time series (gray line = spectrum of 342 length time series and black line = spectrum of 433kyr length time series). Identified Milankovich frequencies are marked with thin black lines.

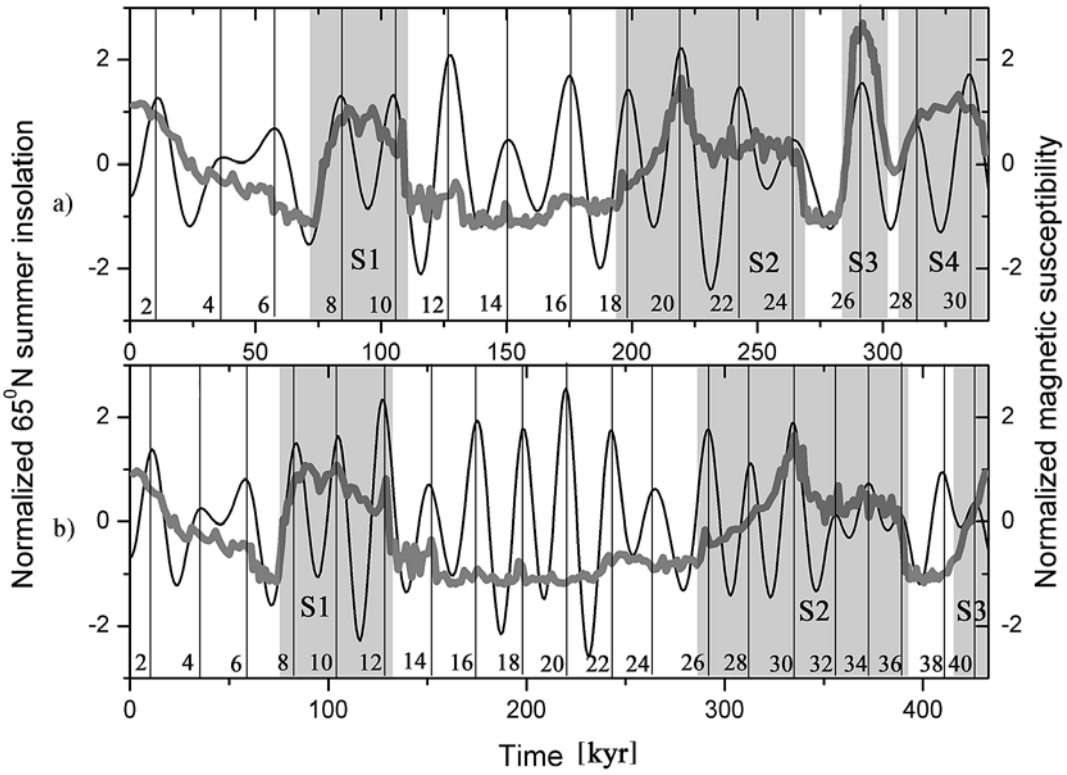

Fig. 3 – Orbital tuned time series for magnetic susceptibility superposed on 65°N summer insolation curves (black line = insolation curves, thick gray line = time series of magnetic susceptibility): (a) 342kyr length curves, (b) 433kyr length curves. The paleosols units are marked by gray regions. The i-cycles of insolation are marked by black thin lines.

insolation curves if we take into account that the paleosols must be correlated with interglacial intervals. Using the i-cycles codification of [26], the interglacial periods in the last 433 ka correspond to i-cycles 7–13 (paleosol S1), 17–23 (paleosol S2), 25–31 (paleosol S3) and 33–39 (paleosol S4). Both target curves failed to correlate correctly all the 4 paleosols.

Spectral analysis (Fig. 2b) shows that the main Milankovich periodicities are present in both time series of the magnetic susceptibility with small differences between them. Thus, the 433 kyr time series have the amplitude associated with the eccentricity slightly shifted to 119kyr and the amplitudes associated with precession and obliquity are smaller compared with those of 342kyr time series. Another feature, common to both time series, is that the amplitudes of orbital frequencies are comparable in magnitude. This result is in contradiction with the majority of paleoclimatic proxies which shows a strong dominance for eccentricity frequency for the last 800 kyr.

This second numerical experiment has produced unreliable results showing that a good orbital tuning cannot be obtained without imposing constrains.

3.2. CORRELATION WITH BENTHONIC $\delta^{18}O$

The resulted depth-time curves of time series obtained through correlation with stack of 57 globally distributed benthic $\delta^{18}O$ records [16] show, as well as for orbital tuning, that the 342 and 417 kyr length time series fit all the IRSL ages (Fig. 4).

With the unforced program the time-depth curves are perfectly superposed, (Fig. 5a) the 342 kyr length curves being continued by the 433 kyr curve placing thus the onset of loess accumulation for Mostistea section at around 433 kyr. The stack of $\delta^{18}O$ was also cut at the age of 433kyr for the reason highlighted for the insolation tuning.

The correlation curves display a good matching between S1 and MIS 5, S2 and MIS 7 and S3 and MIS 9 for both 342 and 433kyr curves testifying that, indeed, these paleosols were developed in interglacial periods, according to the IRSL results (Fig. 6). For 342 kyr length curve the matching program has cut the magnetic susceptibility curve until the base of S3 paleosol confirming again that this paleosol was developed in the interglacial times corresponding to MIS 9 (Fig. 6a). For 433 kyr length curve, S4 was associated with MIS 11 interglacial demonstrating once more that the age of Mostistea sequence is 433 kyr (Fig. 6b).

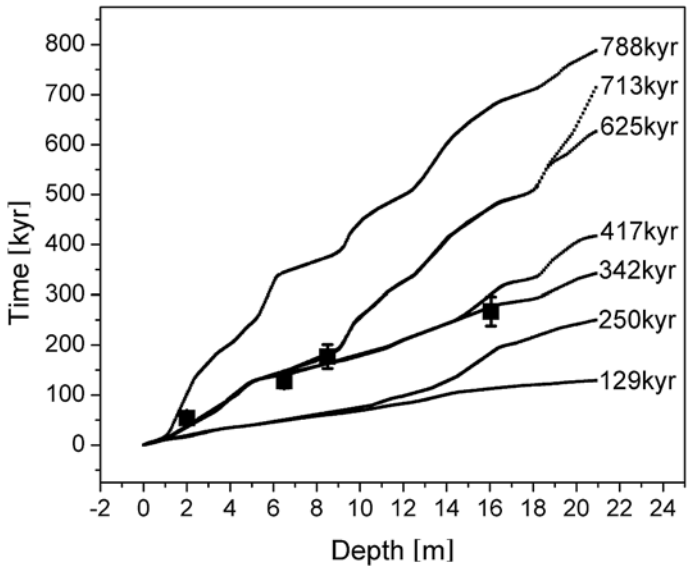

Fig. 4 – Comparison of oxygen matched time series (black lines) and IRSL ages (black squares) with confidence limits.

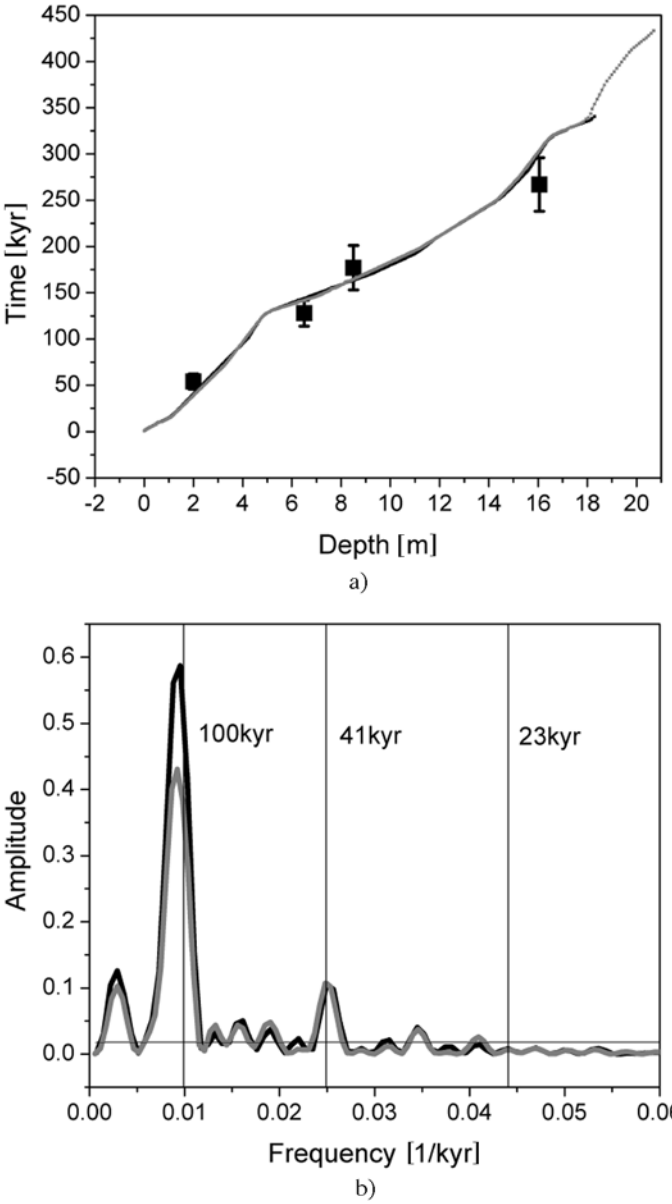

Fig. 5 – (a) Comparison between the two time scales (black line = 342kyr length time series, gray line = 433 length time series) obtained with the unforced program and IRSL ages (black squares) with confidence limits. (b) Power spectra of the same time series (gray line = spectrum of 342 length time series, black line = spectrum of 433kyr length time series).

The spectral analysis displays clearer spectra than for time series obtained through correlation with insolation and a dominant 100kyr eccentricity period (Fig. 5b). Meantime, we observed the lack of precession periodicities above the confidence level which demonstrate that the 23 and 19 kyr periodicities are induced by the insolation. This absence of precession periodicities maybe describe the real case because the time resolution of Mostistea section is very low both in paleosol

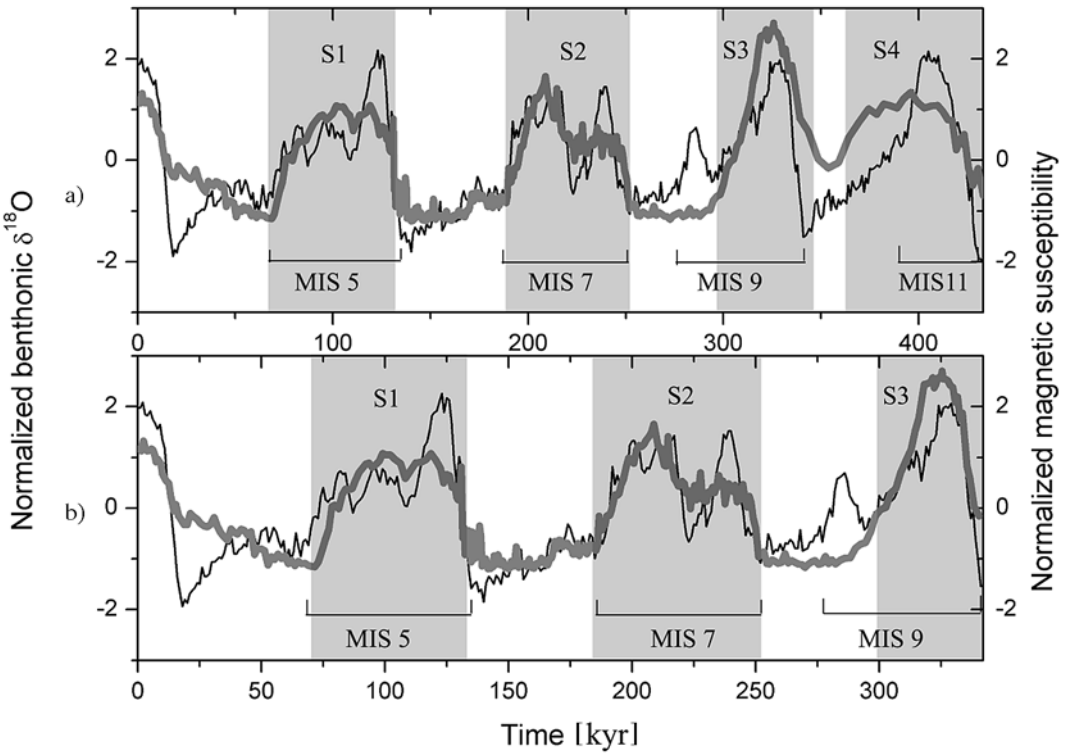

Fig. 6 – Oxygen matched time series superposed on the stack of benthic $\delta^{18}O$ (black line = $\delta^{18}O$ curves, thick gray line = time series of magnetic susceptibility): (a) 342kyr length curves, (b) 433kyr length curves. The paleosols units are marked by gray regions.

and loess layers as can be seen in the magnetic susceptibility variations. Hence, neither paleosol nor loess units record clearly short climatic cycles such as the precession related oscillations. The power spectra for both time series are approximately superposed, with the amplitude corresponding to a 100 kyr periodicity of 342 kyr length curve being greater than that of 433 kyr length time series.

Wavelet analysis for unforced 433 kyr length time series of magnetic susceptibility displays a dominant and continuous band for 100 kyr oscillations, and a 41 kyr period which has also a continuous but more variable shape (Fig. 7). Beginning at around 300 kyr, some kind of continuous leakage effect is observed in all periods of the spectrum. This is because, probably, the S3 paleosol was developed in the entire MIS 9 interglacial and must be correlated as such.

3.3. CORRELATION WITH TIE POINTS

We have generated two time series, one by orbital tuning and the other by correlation of magnetic susceptibility with 57 globally distributed benthic $\delta^{18}O$

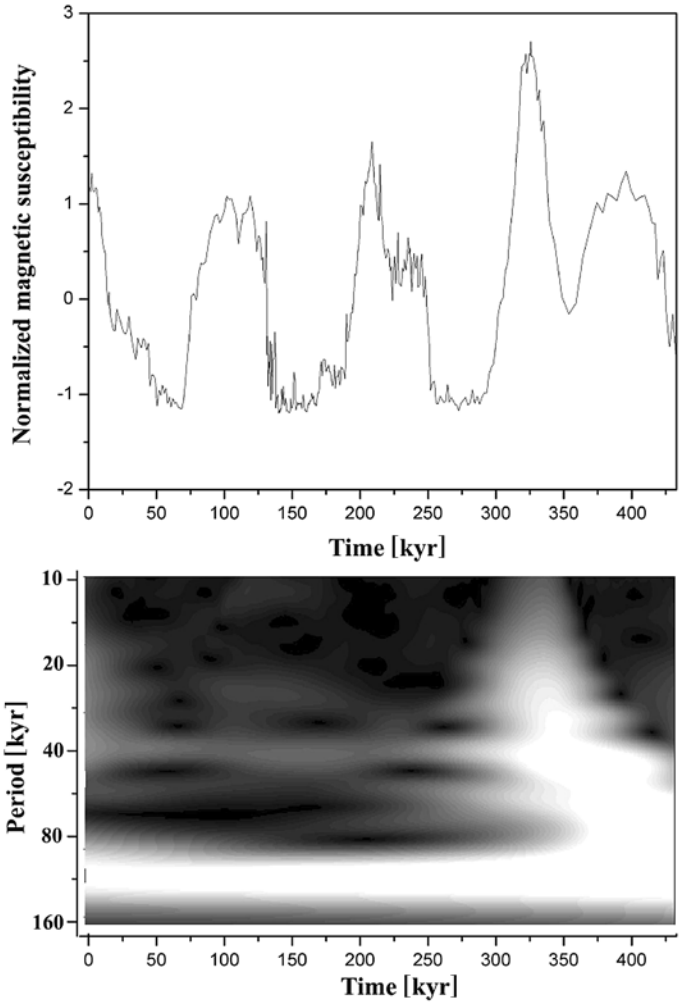

Fig. 7 – Wavelet analysis for unforced 433kyr oxygen matched time series of magnetic susceptibility.

records with tie points. The tuning with insolation procedure adopted follow the scheme used by [2]: paleosols were related to regional maxima in insolation while loess units were assigned to insolation minima. The method utilized a zero time lag between insolation forcing and response of magnetic susceptibility. Because, as we can seen above, the matching program did not correctly associate paleosols to i-cycles which define the interglacials, we need to chose a number of 23 correlation points between our susceptibility record and insolation curve (Fig. 8a).

For the correlation with benthonic oxygen, as the wavelet analysis indicated, the S3 paleosol must be correlated with the entire MIS 9 interglacial. Therefore, we assigned the top of S3 to the top of MIS 9, the base of S3 to the base of MIS 9, and the two maxima of MIS 9 was attributed to the two maxima of S3. In order to a better constrain for S4 we have also associated a two maxima from this paleosol

with corresponding maxima in MIS 11 (Fig. 8b). We considered, as well as for tuning method, a zero time lag between the magnetic susceptibility and benthonic oxygen. The resulted time-depth curves closely resembling, fitting all of the IRSL age points.

Spectral analysis show again a clearer spectrum for the oxygen matched time series than for the orbital tuned one (Fig. 9b). We also note that the precession related oscillations is missing from the spectrum of oxygen matched time series. The powers centered at about 100ka and 41ka are roughly similar with a little

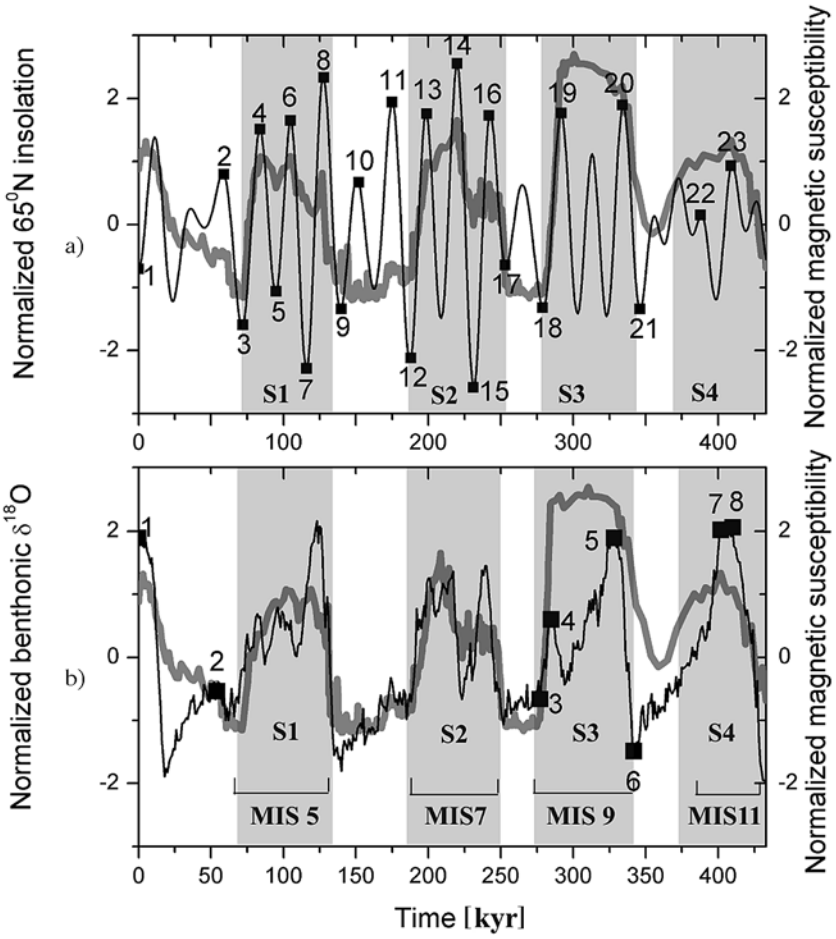

Fig. 8 – (a) Oxygen matched time series superposed on the stack of benthic $\delta^{18}O$ (black line = $\delta^{18}O$ curves, thick gray line = time series of magnetic susceptibility). (b) Orbital tuned time series for magnetic susceptibility superposed on 65°N summer insolation curves (black line = insolation curves, thick gray line = time series of magnetic susceptibility). Correlation points are figured with black squares. Paleosol units are marked by gray regions.

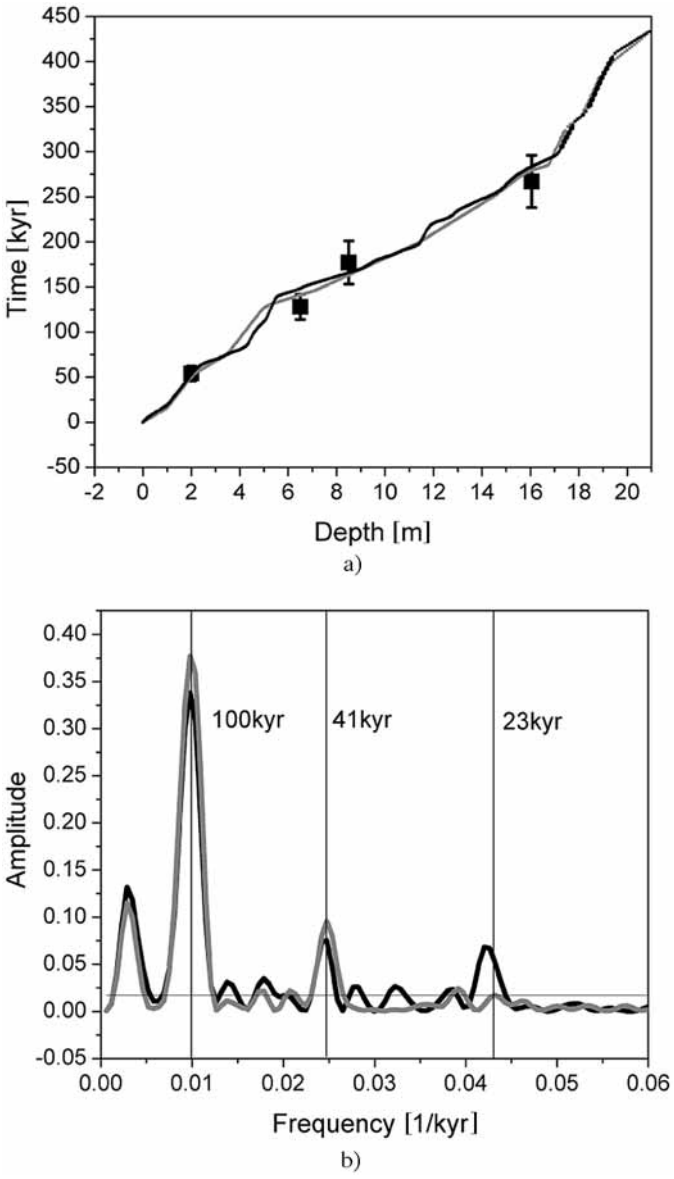

Fig. 9 – (a) Comparison between the oxygen matched (gray line), orbital tuned (black line) time series with tie points and IRSL ages (black squares) with confidence limits. (b) Power spectra of the same time series (gray line = oxygen matched time series, black line = spectrum of orbital tuned time series). Identified Milankovich frequencies are marked with thin black lines.

increase for the oxygen matched time series in both amplitudes. All these suggest that magnetic susceptibility response is more influenced by global ice volume rather than insolation forcing.

The wavelet spectrum of orbital tuned time series show that the 100 kyr eccentricity related period is dominant in the last 433 kyr having a continuous band shape (Fig. 10a). The obliquity period is more variable and presents significant reduction over the time interval of about 150–250 kyr. Precession cycles exhibit a

cluster between 40 and 130 kyr probably caused by an interaction of 19 and 23 kyr periods [27]. This time interval corresponds to the deposition of the second half of the L1 loess unit and to the formation of the S1 paleosol, this part of the Mostistea section having a higher time resolution. A new precession signal appears between 160 and 350 kyr, which corresponds to S2, L3 and S3 units, but without a beating pattern, because time resolution is lower in this part of the Mostistea sequence.

The oxygen matched time series exhibits a little different wavelet spectrum (Fig. 10b). The 100 kyr period, similar to orbital tuned time series, dominates the entire history of loess deposition from Mostistea. The continuous band shape of

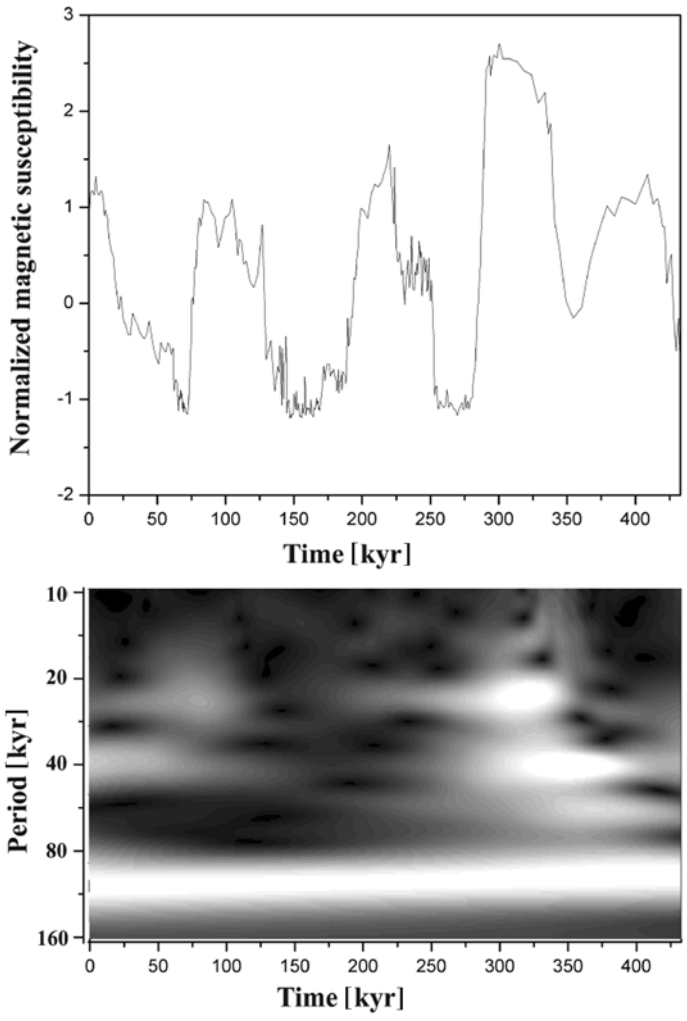

a)

Fig. 10a

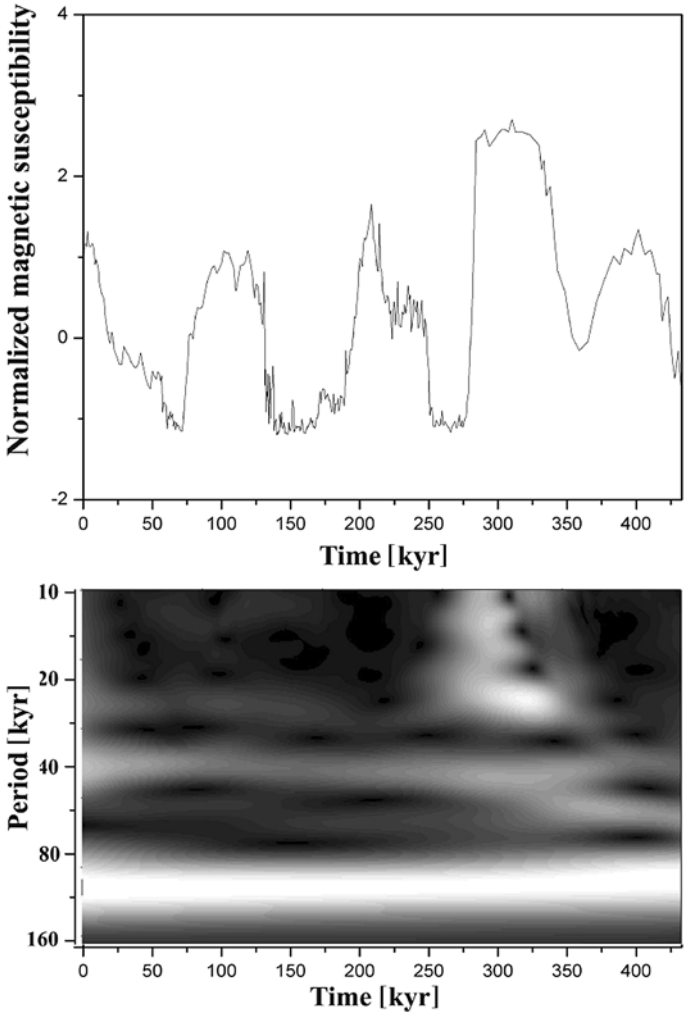

b)

Fig. 10 – Wavelet analysis for (a) orbital tuned time series with tie points and (b) oxygen matched time series with tie points of magnetic susceptibility record from Mostistea loess sequence.

this period also resembles those of the orbital tuned time series. But the 41 kyr obliquity related oscillation shows, unlike the orbital tuned time series, a continuous pattern for the last 433 kyr, distinction which cannot be detected in spectral analysis. The precession signal is very weak indicating that the correlation with the benthonic oxygen curve provides a time series for magnetic susceptibility with a lower time resolution than the orbital tuning method. Thus, it is obvious that the choice of the target curve has a significant effect upon the derived time series both in the spectral and in the time-frequency domain.

4. CONCLUSIONS

The correlation with the stack of 57 globally distributed benthic $\delta^{18}O$ records [16], is more adequate and more intuitive than the orbital tuning for obtaining a time scale for magnetic susceptibility records. This method also suggests that, undoubtedly, even without any constrains, the paleosols developed in interglacials periods, confirming thus the IRSL results. The wavelet analysis has shown that for obtaining a more accurate time scale it is needed to introduce a few tie points, between our signal and the target curve, but much lesser than for orbital tuning. Thus, wavelet analysis is an important tool for detecting such mismatches.

The spectral analysis has shown that the precession signal was induced by insolation tuning, and may not describe a real situation, because the time resolution of our magnetic susceptibility records is very weak. Therefore, one more time, the correlation with the benthonic $\delta^{18}O$ curve seems to be more straightforward. Wavelet analysis has shown that, for precession and obliquity periods, time-frequency distributions are different for orbital tuned and oxygen matched time series proving that different target curves provide time scales with different spectral properties. We also want to point out that wavelet analysis can detect differences in orbital frequencies which cannot be seen in classical spectral analysis.

The good correlation between magnetic susceptibility and benthonic $\delta^{18}O$ testifies that a major contribution upon magnetic susceptibility variations come from the late Quaternary growths and decays of the global ice volume and only a small part of the magnetic susceptibility response is caused by insolation forcing.

REFERENCES

1. H. Lu, X. Liu, F. Zhang, Z. An, J. Dodson, *Astronomical calibration of loess-paleosol deposits at Luochuan central Chinese loess plateau*, Plaeogoegraphy, Plaeoclimatology, Paleoecology, 154, 237–246, 1999.
2. D. Heslop, C. G. Langereis, M. J. Dekkers, *A new astronomical time scale for the loess deposits of Northern China*. Earth and Planetary Science Letters 184, 125–139, 2000.
3. Z. L. Ding, V. Ranov, S. L. Yang, A. Finaev, J. M. Han., G. A. Wang, *The loess record in southern Tajikistan and correlation with Chinese loess*. Earth and Planetary Science Letters, 200, 387–400, 2002.
4. Y. Sun, S. C. Clemens, Z. An, Z. Yu, *Astronomical time scale and palaeoclimatic implication of stacked 3.6-Myr monsoon records from the Chinese Loess Plateau*. Quaternary Science Reviews, in press, 2005.
5. J. Imbrie, *et al.*, *On the structure and origin of major glaciation cycles. 2. The 100,000-year cycle*. Paleoceanography, 8, 699–735, 1993a.
6. N. J. Shackleton, *The 100,000-year ice-age cycle identified and found to lag temperature, carbon dioxide and orbital eccentricity*. Science, 289, 1897–1902, 2000.
7. D. Karner, R. Muller, *A causality problem for Milankovich*, Science, 288, 2143–2144, 2000.
8. M. Elkibbi, J. Rial, *An outsider's review of the astronomical theory of theclimate: Is the eccentricity driven insolation the main driver of the ice ages?*, Earth Sci. Rev., 56, 161–177, 2001.

9. C. Wunsch, *The spectral description of climate change including 100 ky energy*. Climate Dynamics, 20, 353–363, 2003a.
10. C. Wunsch, *Quantitative estimate of the Milankovich-forced contribution to observed Quaternary climate change*, Quaternary Science Reviews, 23, 1001–1012, 2004 .
11. Y. Ashkenazy, E. Tziperman, *Are the 41 kyr glacial oscillations a linear response to Milankovich forcing?*, Quaternary Science Reviews, 23, 1879–1890, 2004.
12. P. Huybers, C. Wunsch, *A depth-derived Pleistocene age model: Uncertainty estimates, sedimentation variability, and nonlinear climate change*, Paleoceanography, 19, PA1028, doi:10.1029/2002PA000857, 2004 .
13. C. G. Panaiotu, E. C. Panaiotu, A. Grama, C. Necula, *Paleoclimatic record from a loess-paleosol profile in southeastern Romania*. Physics and Chemistry of the Earth 26, 893–898, 2001.
14. C. E. Panaiotu, S. Balescu, M. Lamothe, C. G. Panaiotu, C. Necula, A. Grama, *Astronomical and luminescence dating of lower Danubian loess (Romania)*, Geophysical Research Abstracts, Vol. 6, 02900, 2004.
15. A. Berger, M. F. Loutre, *Insolation values for the climate of the last 10 million years*. Quaternary Science Reviews 10, 291–317, 1991 .
16. L. E. Lisiecki, M. E. Raymo, *A Pliocene-Pleistocene stack of 57 globally distributed benthic $\delta^{18}O$ records*, Paleoceanography, 20, PA1003, doi:10.1029/2004PA001071, 2005.
17. L. E. Lisiecki, P. A. Lisiecki, *Application of dynamic programming to the correlation of paleoclimate records*, Paleoceanography, 17 (4), 1049, doi:10.1029/2001PA000733, 2002.
18. J. Laskar, F. Joutel, F. Boudin, *Orbital, precessional and insolation quantities for the Earth from –20 Myr to +10 Myr*, Astron. d Astrophys., 270, 522–533, 1993.
19. M. Schulz, K. Stattegger, *SPECTRUM: spectral analysis of unevenly spaced paleoclimatic time series*. Computers & Geosciences Vol. 23, No. 9, pp. 929–945, 1997.
20. A. Mathias, F. Grond, R. Guardans, D. Seese, M. Canela, H. H. Diebner, *Algorithms for spectral analysis of irregularly sampled time series*, Journal of Statistical Software, Vol. 11, Issue 2, 1–27, 2004.
21. J. Navroki, V. Bakhumutov, A. Boguchi, L. Dolechi, *The paleo-petromagnetic record in the Polish and Ukrainian loess-paleosol sequences*, Phys. Chem. Earth, 24, 9, 773–777, 1999.
22. A. Tsatskin, F. Heler, T. S. Gendler, E. I. Virina, S. Spassov, J. Du Pasquier, J. Hus, E. A. Hailwood, V. I. Bagin, S. S. Faustov, *A new scheme of terrestrial paleoclimate evolution during the last 1.5 My in the western Black Sea region: a integration of soil and loess magnetism*, Phys. Chem. Earth, 26, 11–12, 911–916, 2001.
23. D. Jordanova, N. Petersen, *Paleoclimatic record from a loess soil profile in northeastern Bulgaria-II. Corelation with global climatic events during the Pleistocene*, Geophys. J. Int., 138, 533–540, 1999b.
24. M. Sartori, F. Heller, T. Forster, M. Borkovec, J. Hammann, E. Vincent, *Magnetic properties of loess grain size fractions from the section at Paks (Hungary), Phys. Earth. Platen. Inter.*, 116, 53–64, 1999.
25. D. Heslop, M. J. Dekkers, C. G. Langereis, *Timing and structure of the Mid-Pleistocen transition: records from the loess deposits of northern China*. Paleogeography, Paleoclimatology, Paleoecology, 185, 133–143, 2002.
26. L. J. Lourens, A. Antonarakou, E. J. Hilgen, A. A. M. van Hoof, C. Vergnaud-Grazzini, W. J. Zachariasse, *Evaluation of the Plio-Pleistocene astronomical timescale*, Paleoceanography, 11, 391–413, 1996.
27. E. W. Bolton, K. Maasch, J. M. Lilly, *A wavelet analysis of Plio-Pleistocene climate indicators: A new view of periodicity evolutions*. Goephysical Research Letters, Vol. 22, No. 20, 2753–2756, 1995.